

Simulation of Water-Soil-Structure Interactions Using Incompressible Smoothed Particle Hydrodynamics

Abdelraheem M. Aly^{1,2,*}, Mitsuteru Asai³ and Ehab Mahmoud Mohamed^{4,5}

Abstract: In the present work, an incompressible smoothed particle hydrodynamic (SPH) method is introduced to simulate water-soil-structure interactions. In the current calculation, the water is modelled as a Newtonian fluid. The soil is modelled in two different cases. In the first case, the granular material is considered as a fluid where a Bingham type constitutive model is proposed based on Mohr-Coulomb yield-stress criterion, and the viscosity is derived from the cohesion and friction angle. In addition, the fictitious suspension layers between water and soil depending on the concentration of soil are introduced. In the second case, Hooke's law introduces elastic soil. In ISPH, the pressure is evaluated by solving the pressure Poisson equation using a semi-implicit algorithm based on the projection method and an eddy viscosity for water is modelled by a large eddy simulation with the Smagorinsky model. In the proposed ISPH method, the pressure is stabilized to simulate the multiphase flow between soil and water. Numerical experiments for water-soil suspension flow of Louvain erosional dam break with flat soil foundation, is simulated and validated using 3D-ISPH method. Coupling between water-soil interactions with different solid structures are simulated. The results revealed that, the suspension layers with the Bingham model of soil gives more accurate results in the experiment as compared to the case of the Bingham model without suspension layers. In addition, the elastic soil model by the Hooke's law can simulate soil hump accurately as compared to the Bingham model. From the simulations, avoiding erosion behind the structure for preventing the structure break during flood are investigated by using an extended structure or a wedge structure.

Keywords: Bingham model, ISPH method, rigid body, water-soil interactions.

¹ Department of Mathematics, College of Science, King Khalid University, Abha, 62529, Saudi Arabia.

² Department of Mathematics, Faculty of Science, South Valley University, Qena, 83523, Egypt.

³ Civil Engineering Department, Kyushu University, Fukuoka, 819-0395, Japan.

⁴ Electrical Engineering Department, College of Engineering, Prince Sattam Bin Abdulaziz University, Wadi Addwasir, 11991, Saudi Arabia.

⁵ Electrical Engineering Department, Faculty of Engineering, Aswan University, Aswan, 81542, Egypt.

* Corresponding Author: Abdelraheem M. Aly. Email: abdelreheam.abdallah@sci.svu.edu.eg.

Received: 24 November 2019; Accepted: 09 March 2020.

1 Introduction

The interaction between water, soil and structures poses problems to different areas of marine, geomechanics and hydraulic engineering. Numerical predictions for such interactions in the case of large deformations could provide useful knowledge for engineering practice and design. There are some traditional numerical methods for deformation and failure of geomaterials in the framework of continuum mechanics, such as Finite Element Method (FEM), Finite Difference Method (FDM) and Boundary Element Method (BEM). These methods have been successfully implemented. On the other hand, in the case of large deformation problems, the previous methods produce instabilities due to excessive distortion of a mesh. Several numerical methods have been introduced for large deformation problems. A more general method is the smoothed particle hydrodynamics (SPH) method, originally proposed by Lucy [Lucy (1977)] and further developed by Gingold et al. [Gingold and Monaghan (1977)] for treating astrophysical problems. Its main advantage is the absence of a computational grid or mesh since it is spatially discretized into Lagrangian moving particles. This allows the possibility of easily modelling flows with a complex geometry or flows where large deformations or the appearance of a free surface occurs. At the present time, it is being exploited for the solution of problems appearing in different physical processes. Monaghan [Monaghan (1992)] has provided a fairly extensive review of SPH methods. The SPH method was applied into compressible and incompressible viscous flow problems [Monaghan (1994); Morris, Fox and Zhu (1997); Monaghan (1995); Okahci, Hirota, Izawa et al. (2001)]. The SPH was originally developed in compressible flow, then some special treatment was required to satisfy the incompressible condition. One approach is to run the simulations in the quasi-incompressible limit, that is by selecting the smallest possible speed of sound which still gives a very low Mach number ensuring density fluctuations within 1% [Monaghan (1994); Morris, Fox and Zhu (1997)]. This method is known as the Weakly Compressible Smooth Particle Hydrodynamics (WCSPH). In the WCSPH, the artificial viscosity, which is originally developed by Monaghan [Monaghan (1992)], has been widely used not only for the energy dissipation but also for preventing unphysical penetration of particles. Recently a proposal for constructing an incompressible SPH model has been introduced, where pressure is implicitly calculated by solving a discretized pressure Poisson equation at every time step [Cummins and Rudman (1999); Pozorski and Wawrenczuk (2002); Shao and Lo (2003); Hu and Adams (2006); Ellero, Serrano and Espanol (2007); Lee, Moulinec, Xu et al. (2008); Khayyer, Gotoh and Shao (2008); Khayyer, Gotoh and Shao (2009); Hu and Adams (2007); Hu and Adams (2009)].

On the other hand, SPH method has been developed for solving large deformation and post failure flow of soil [Bui, Sako and Fukagawa (2007); Bui, Fukagawa, Sako et al. (2008); Bui and Fukagawa (2013); Pastor, Haddad, Sorbino et al. (2009)]. In the water-saturated soil problem, Bui et al. [Bui, Sako and Fukagawa (2007)] modelled the dry soil by one phase flow while saturated soil is modelled by separate water and soil phases and the interaction between soil and water is taken into account by means of pore water pressure and seepage force. Bui et al. [Bui and Fukagawa (2013)] showed that, it is common in computational geomechanics to treat the two phase system as a single phase with the interaction between soil and water handled by adding the pore-water pressure to

the effective stress, that is Terzaghi's concept of effective stress. They used this approach to model the saturated soil problem with SPH method. On the other hand, Ulrich et al. [Ulrich, Koliha and Rung (2011)] modelled the water/soil interaction by SPH method as a multiphase flow and the layers between water and soil are introduced as fictitious suspension layers, which deserve more attention in several cases. In the current work, we follow Ulrich et al.'s [Ulrich, Koliha and Rung (2011)] technique for treating the interaction between water, soil and suspension layers. The fluids are assumed to be Newtonian and an eddy viscosity is modelled by means of large eddy simulation using the Smagorinsky model. The soil model considers the granular material as a fluid where a Bingham type constitutive model is proposed based on Mohr-Coulomb yield-stress criterion and the viscosity is derived from the cohesion and friction angle. A concentration based approach to mimic the stresses inside the fictitious suspension layer is introduced which is derived from a Chezy-relation between the shear stresses and the local flow velocity as proposed by Fraccarollo et al. [Fraccarollo and Chapart (2002)].

Recently, Ren et al. [Ren, Zhuang, Rabczuk et al. (2019)] derived dual-support SPH (DS-SPH) in the field of solid mechanics. The main advantage of DS-SPH method is the easy formulation of tangent stiffness matrix. Dai et al. [Dai, Ren, Zhuang et al. (2017)] introduced different support domain and dual-support of SPH method for treating elastic mechanics. Ren et al. [Ren, Zhuang and Rabczuk (2019)] developed dual-support smoothed particle hydrodynamics (DS-SPH) method with variable smoothing length. The current DS-SPH is applied into weakly compressible flow including water droplet flow and 2D dam break over dry bed. It is reported that DS-SPH can reduce the computational cost compare to conventional SPH.

Ren et al. [Ren, Zhuang and Rabczuk (2017)] presented the dual-horizon peridynamics (DH-PD) formulation for simulations of crack paths with variable horizon and particle sizes. Ren et al. [Ren, Zhuang, Cai et al. (2016)] developed dual-horizon peridynamics which includes variations on the horizon sizes. Rabczuk et al. [Rabczuk, Ren and Zhuang (2019)] proposed the novel nonlocal operator theory based on the vibrational principle for solving the partial differential equations. The novel nonlocal operator can stabilize meshes methods by the dual-concept and allows implementation of complete implicit methods.

In the present study, the pressure is stabilized by introducing the source term which contains both contributions from velocity-divergence free and density invariance conditions [Aly, Asai and Sonoda (2011a, 2011b); Asai, Aly, Sonoda et al. (2012)]. In addition, the eddy viscosity based on the Smagorinsky model is introduced.

To simulate soil hump for seawall, Bingham flow approach with suspension region and solid approach for soil, are integrated, then the technique is applied to a seawall collapse simulation during a tsunami. The modification in the original Bingham flow model [Ulrich, Koliha and Rung (2011)], which is based on weakly compressible approach for water, is the extension to the incompressible formulation by ISPH. First, the water-soil suspension flow of Louvain erosional dam break [Fraccarollo and Chapart (2002)] with flat soil foundation is simulated using 3D-ISPH method. This simulation is validated by comparing it to the experimental results. Second, several numerical tests for fluid-structure soil foundation interactions are discussed.

2 Mathematical analysis

The governing equations of transient compressible fluid flow include the equations for conservation of mass and momentum are:

$$\frac{1}{\rho} \frac{D\rho}{Dt} + \frac{\partial \mathbf{v}^\alpha}{\partial x^\alpha} = 0, \quad (1)$$

$$\frac{D\mathbf{v}^\alpha}{Dt} = \frac{1}{\rho} \frac{\partial \sigma^{\alpha\beta}}{\partial x^\beta} + \mathbf{g}^\alpha, \quad (2)$$

where subscripts α and β refer to the spatial coordinates, t is the time, \mathbf{g} is the gravitational acceleration, \mathbf{v} is the velocity vector.

2.1 Fluid model

For the simple Newtonian fluids, the stress tensor σ is given by:

$$\sigma^{\alpha\beta} = -p\delta^{\alpha\beta} + \tau^{\alpha\beta}, \quad (3)$$

where p is the pressure, $\delta^{\alpha\beta}$ is the unit tensor and $\tau^{\alpha\beta}$ is the stress tensor and represents the viscous stresses which depend on an isotropic viscosity μ^* and gradient of velocity as:

$$\tau^{\alpha\beta} = \mu^* \left(\frac{\partial \mathbf{v}^\beta}{\partial x^\alpha} + \frac{\partial \mathbf{v}^\alpha}{\partial x^\beta} \right) + \mathcal{G} \left(\frac{\partial \mathbf{v}^\gamma}{\partial x^\gamma} \right) \delta^{\alpha\beta}, \quad (4)$$

where, \mathcal{G} is viscosity coefficient and strain rate-tensor is defined as:

$$S^{\alpha\beta} = \frac{1}{2} \left(\frac{\partial \mathbf{v}^\beta}{\partial x^\alpha} + \frac{\partial \mathbf{v}^\alpha}{\partial x^\beta} \right), \quad (5)$$

And the effective dynamic viscosity μ^* is composed from a viscosity μ and an eddy viscosity μ_T as:

$$\mu^* = \mu + \mu_T \quad (6)$$

In this paper, it is assumed that the eddy viscosity is modeled by the static Smagorinsky model as $\mu_T = \rho (C_s \Delta)^2 |\bar{S}|$, in which $C_s = 0.2$ is the Smagorinsky constant (taken as the analytical value in this paper), Δ is constant and it taken as smoothing compact support. The local strain rate $|\bar{S}| = (2\bar{S}^{\alpha\beta}\bar{S}^{\alpha\beta})^{1/2}$ can be calculated in the SPH formulation as Violeau et al. [Violeau and Issa (2007)].

For incompressible fluids $\nabla \cdot \mathbf{v} = 0$; the viscous stress tensor is:

$$\tau^{\alpha\beta} = \mu_f^* \left(\frac{\partial \mathbf{v}^\beta}{\partial x^\alpha} + \frac{\partial \mathbf{v}^\alpha}{\partial x^\beta} \right), \quad (7)$$

The total stress tensor is therefore:

$$\sigma^{\alpha\beta} = -p\delta^{\alpha\beta} + \mu_f^* \left(\frac{\partial v^\beta}{\partial x^\alpha} + \frac{\partial v^\alpha}{\partial x^\beta} \right), \quad (8)$$

Note that, in the most general incompressible flow approach, the density is assumed by a constant value with its initial value ρ^0 . Then, the governing equations for an incompressible Newtonian fluid are summarized:

$$\frac{D\rho}{Dt} = 0, \quad (\text{incompressibility}) \quad (9)$$

$$\frac{\partial v^\alpha}{\partial x^\alpha} = 0, \quad (\text{continuity}) \quad (10)$$

$$\frac{Dv^\alpha}{Dt} = -\frac{1}{\rho^0} \frac{\partial p}{\partial x^\alpha} + \frac{1}{\rho^0} \frac{\partial}{\partial x^\beta} \left(\mu_f^* \left(\frac{\partial v^\beta}{\partial x^\alpha} + \frac{\partial v^\alpha}{\partial x^\beta} \right) \right) + g^\alpha, \quad (\text{momentum}) \quad (11)$$

2.1.1 Projection method

In the projection method [Cummins and Rudman (1999)], the velocity-pressure coupling problem has been solved separately for velocity and pressure. Here, all the state variables may update from a previous time step to current time step. In this below, superscripts (n) and ($n+1$) indicate previous and current time step, respectively. In the first predictor step, the intermediate distate without pressure gradient is assumed and its velocity field is indicated by \mathbf{v}^* . The intermediate velocity field can be evaluated by solving the following equation:

$$\frac{\mathbf{v}_*^\alpha - \mathbf{v}_n^\alpha}{\Delta t} = \frac{1}{\rho^0} \frac{\partial}{\partial x^\beta} \left(\mu_f^* \left(\frac{\partial v_n^\beta}{\partial x^\alpha} + \frac{\partial v_n^\alpha}{\partial x^\beta} \right) \right) + g^\alpha, \quad (12)$$

$$(\text{Predictor}): \mathbf{v}_*^\alpha = \mathbf{v}_n^\alpha + \Delta t \left(\frac{1}{\rho^0} \frac{\partial}{\partial x^\beta} \left(\mu_f^* \left(\frac{\partial v_n^\beta}{\partial x^\alpha} + \frac{\partial v_n^\alpha}{\partial x^\beta} \right) \right) + g^\alpha \right) \quad (13)$$

Then, the following corrector step introduces an effect of remaining 'current' pressure gradient term as follow:

$$\frac{\mathbf{v}_{n+1}^\alpha - \mathbf{v}_*^\alpha}{\Delta t} = -\frac{1}{\rho^0} \frac{\partial p_{n+1}}{\partial x^\alpha}, \quad (14)$$

$$(\text{Corrector}): \mathbf{v}_{n+1}^\alpha = \mathbf{v}_*^\alpha + \Delta \mathbf{v}_*^\alpha = \mathbf{v}_*^\alpha - \Delta t \left(\frac{1}{\rho^0} \frac{\partial p_{n+1}}{\partial x^\alpha} \right), \quad (15)$$

where $\Delta \mathbf{v}_*^\alpha$ indicates the incremental velocity from the predicted velocity \mathbf{v}_*^α .

The key point here is the evaluation of 'current' pressure value. By taking the divergence of correction step (Eq. (14)) as:

$$\frac{\partial}{\partial x^\alpha} \left(\frac{\mathbf{v}_{n+1}^\alpha - \mathbf{v}_*^\alpha}{\Delta t} \right) = -\frac{\partial}{\partial x^\alpha} \left(\frac{1}{\rho^0} \frac{\partial p_{n+1}}{\partial x^\alpha} \right), \quad (16)$$

From the incompressible condition (Eq. (9)), which leads:

$$\frac{\partial \mathbf{v}_{n+1}^\alpha}{\partial x^\alpha} = 0, \quad (17)$$

By substitute Eqs. (17) into (16), this leads to the following pressure Poisson equation (PPE):

$$\frac{\partial}{\partial x^\alpha} \left(\frac{1}{\rho^0} \frac{\partial p_{n+1}}{\partial x^\alpha} \right) = \frac{\rho^0}{\Delta t} \frac{\partial \mathbf{v}_*^\alpha}{\partial x^\alpha} + \gamma \frac{\rho^0 - \rho^{num}}{\Delta t^2}, \quad (18)$$

where, $\gamma: (0 \leq \gamma \leq 1)$ is a relaxation coefficient and ρ^{num} is the numerical density, which is calculated from SPH approximation.

The above corrector step can be implemented by substituting the pressure gradient with the solution of PPE. The flow chart for solving steps of fluid flow using ISPH method has been introduced in Fig. 1.

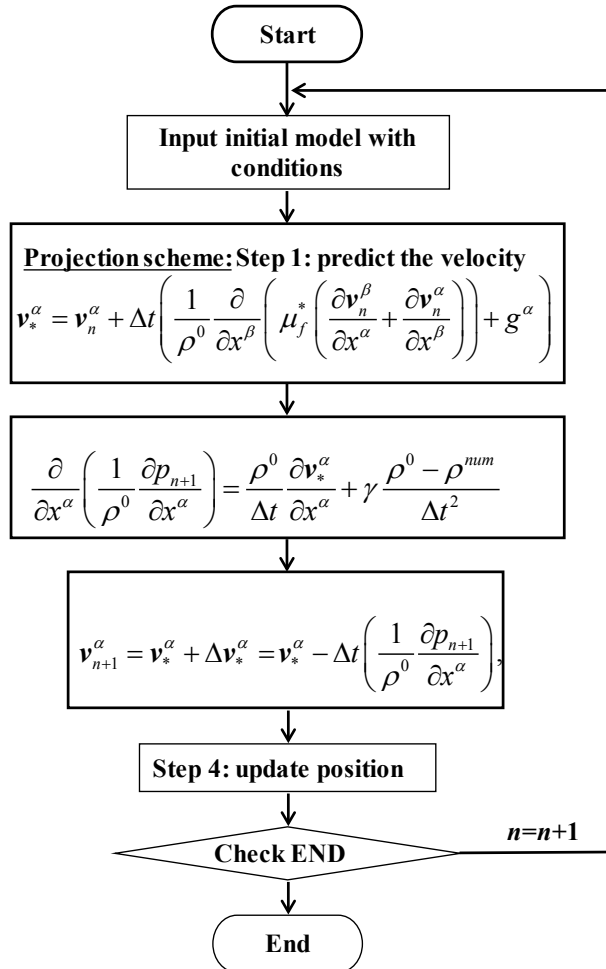


Figure 1: Flow chart of ISPH method for fluid flow model

2.2 Soil model

In this section, the two different approaches of soil modelling are discussed. In the first approach, the soil model considers the granular material as a fluid with a variable viscosity, where a Bingham type constitutive model is proposed based on Mohr-Coulomb yield-stress criterion [Ulrich, Koliha and Rung (2011)]. The other approach [Bui, Sako and Fukagawa (2007)] is the use of nonlinear material constitutive model in the framework of solid mechanics.

2.2.1 Bingham flow

Here, the soil particles are treated as a viscous material with a variable viscosity. Where, the viscosity is based on Mohr-Coulomb yield-stress criterion for granular material and is derived as follows:

For non-Newtonian fluids with the yield strength, the relation between shear stress τ and shear strain rate $\dot{\gamma}$ is given by:

$$\tau = \mu_{so} \dot{\gamma} + \tau_y, \quad (19)$$

where, τ_y is the yield shear strength. For shear stresses below the yield stress, a Bingham fluid has behavior such as a rigid body and doesn't deform but when the shear stress surpasses the yield stress, the flow failure occurs resulting in large deformations. Fig. 2 presents the relation between shear stress and shear strain. The Mohr-Coulomb criterion is introduced as the yield shear strength in the Bingham model for a given soil as:

$$\tau_y = c + p \tan \phi \quad (20)$$

where, c is the cohesion, and ϕ is the friction angle. Then, the soil viscosity should be expressed in Bingham model as:

$$\mu_s = \frac{\tau}{\dot{\gamma}} = \begin{cases} \mu_{so} + \frac{c + p \tan \phi}{\dot{\gamma}} & \mu_s < \mu_{s \max} \\ \mu_{s \max} & \mu_s \geq \mu_{s \max} \end{cases} \quad (21)$$

where, μ_{so} is the viscosity after yield, $\mu_{s \max}$ is the maximum viscosity for a given soil.

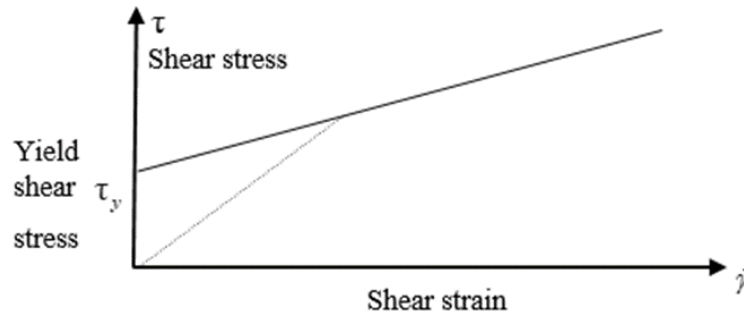


Figure 2: Relation between shear stress and shear strain

2.2.2 Water-soil suspension flow

The suspension layer is nested between soil and water regions depending on the concentration of soil. Particles which reside inside a fictitious suspension layer are assigned to a viscosity that is derived from a Chezy-relation between the stress and the local flow velocity along a route outlined by Fraccarollo et al. [Fraccarollo and Chapart (2002)].

$$\mu_c^* = \frac{\rho_s C_f (v^\alpha v^\alpha)}{\dot{\gamma}} + \mu_T \quad (22)$$

where, ρ_s is the density of soil and C_f is the friction coefficient of the Chezy-relation. Three different regions are defined, depending on the local volumetric soil concentration \tilde{c}_{soil} as:

$$\mu_{susp}^* = \begin{cases} \mu_f^* + \frac{\mu_c^* - \mu_f^*}{0.2} & \tilde{c}_{soil} \leq 0.2 \\ \mu_c^* & 0.2 < \tilde{c}_{soil} < 0.6, \\ \mu_c^* + \frac{\mu_s^* - \mu_c^*}{1-0.6} (\tilde{c}_{soil} - 0.6) & \tilde{c}_{soil} \geq 0.6 \end{cases} \quad (23)$$

2.2.3 Elastic soil

In the current study, the elastic model will be introduced to describe the soil behavior. Hooke's law is used as the constitutive model:

$$\sigma^{\alpha\beta} = D_e^{\alpha\beta\gamma\zeta} \varepsilon_e^{\gamma\zeta} \quad (24)$$

where, $\sigma^{\alpha\beta}$ is the stress tensor, $D_e^{\alpha\beta\gamma\zeta}$ is the elastic modulus matrix. For an elastic model, the resulting constitutive model is typically given by:

$$\dot{\sigma}^{\alpha\beta} = 2G \dot{\varepsilon}^{\alpha\beta} + K \dot{\varepsilon}^{\gamma\gamma} \delta^{\alpha\beta} \quad (25)$$

where, $\dot{\varepsilon}^{\alpha\beta} = \dot{\varepsilon}^{\alpha\beta} - \frac{1}{3} \dot{\varepsilon}^{\gamma\gamma} \delta^{\alpha\beta}$ is the deviatoric shear strain rate tensor; K is the elastic bulk modulus, which relates to the shear modulus G and Poisson's ratio λ through the following equations:

$$K = \frac{E}{3(1-2\lambda)} \quad \text{and} \quad G = \frac{E}{2(1+\lambda)} \quad (26)$$

3 SPH formulation

3.1 SPH concepts

In the SPH method, a physical scalar function $\phi(x_i, t)$ at a sampling point x_i can be represented by:

$$\phi(x_i, t) \approx \langle \phi_i \rangle = \sum_j \frac{m_j}{\rho_j} W(r_{ij}, h) \phi_j(x_j, t), \quad (27)$$

where, the subscripts i and j indicate positions of labeled particle, and m_j means representative mass related to particle j . Note that the triangle bracket $\langle \phi_i \rangle$ means SPH approximation of a function ϕ . W is a weight function called by smoothing kernel function in the SPH literature. In the smoothing kernel function, $r_{ij} = (|x_i - x_j|)$ and h are the distance between neighbor particles and smoothing length, respectively. The divergence of the scalar function can be assumed by using the above defined SPH approximation as follows:

$$\frac{\partial \phi(r_i)}{\partial x^\beta} \approx \langle \frac{\partial \phi_i}{\partial x^\beta} \rangle = \sum_j \frac{m_j}{\rho_j} (\phi_j - \phi_i) \frac{\partial W(r_{ij}, h)}{\partial x^\beta}, \quad (28)$$

Also, the other expression for the gradient can be represented by:

$$\frac{\partial \phi(r_i)}{\partial x^\beta} \approx \langle \frac{\partial \phi_i}{\partial x^\beta} \rangle = \rho_i \sum_j m_j \left(\frac{\phi_j}{\rho_j^2} + \frac{\phi_i}{\rho_i^2} \right) \frac{\partial W(r_{ij}, h)}{\partial x^\beta}. \quad (29)$$

In this paper, quintic spline function is utilized as a kernel function as follows:

$$W(r_{ij}, h) = \beta_d \times \begin{cases} \left(3 - \frac{r_{ij}}{h} \right)^5 - 6 \left(2 - \frac{r_{ij}}{h} \right)^5 + 15 \left(1 - \frac{r_{ij}}{h} \right)^5 & 0 \leq r_{ij} < h \\ \left(3 - \frac{r_{ij}}{h} \right)^5 - 6 \left(2 - \frac{r_{ij}}{h} \right)^5 & h \leq r_{ij} < 2h \\ \left(3 - \frac{r_{ij}}{h} \right)^5 & 2h \leq r_{ij} < 3h \\ 0 & r_{ij} \geq 3h \end{cases}, \quad (30)$$

where, β_d is $7/478\pi h^2$ and $3/358\pi h^3$ in two and three dimension space.

3.2 Discretization of projection method

Here, the projection method for incompressible fluid and Bingham flow problems is discretized into particle quantities based on the SPH methodology. For this purpose, the gradient of pressure and the divergence of velocity are approximated as follow:

$$\frac{\partial p(x_i)}{\partial x^\beta} \approx \langle \frac{\partial p_i}{\partial x^\beta} \rangle = \rho_i \sum_j m_j \left(\frac{p_j}{\rho_j^2} + \frac{p_i}{\rho_i^2} \right) \frac{\partial W(r_{ij}, h)}{\partial x^\beta}, \quad (31)$$

$$\frac{\partial \mathbf{v}^\alpha(x_i)}{\partial x^\beta} \approx \left\langle \frac{\partial \mathbf{v}_i^\alpha}{\partial x^\beta} \right\rangle = \sum_j \frac{m_j}{\rho_j} (\mathbf{v}_j^\alpha - \mathbf{v}_i^\alpha) \cdot \frac{\partial W(r_{ij}, h)}{\partial x^\beta}, \quad (32)$$

The second derivative of velocity for the viscous force and the Laplacian pressure have been proposed by Morris et al. [Morris, Fox and Zhu (1997)] by an approximation expression as follows:

$$\frac{\partial}{\partial x^\beta} \left(\mu_f^* \left(\frac{\partial \mathbf{v}_n^\beta}{\partial x^\alpha} + \frac{\partial \mathbf{v}_n^\alpha}{\partial x^\beta} \right) \right) = \sum_j \frac{m_j}{\rho_j} \left(\frac{(\mu_f^*)_i + (\mu_f^*)_j}{\rho_i \rho_j} \frac{(r_n^{\alpha\beta})_{ij}}{(r_n^{\alpha\beta})_{ij}^2 + \eta^2} \cdot \frac{\partial W_{ij}}{\partial x^\alpha} \right) (\mathbf{v}_n^{\alpha\beta})_{ij}, \quad (33)$$

where η is a parameter to avoid a zero dominator, and its value is usually given by $\eta^2 = 0.0001 h^2$.

Similarly, the Laplacian of pressure in pressure Poisson equation (PPE) is given by:

$$\frac{\partial}{\partial x^\alpha} \left(\frac{1}{\rho^0} \frac{\partial p_{n+1}}{\partial x^\alpha} \right) = \sum_j m_j \left(\frac{\rho_i + \rho_j}{\rho_i \rho_j} \right) \left(\frac{(p_{n+1})_{ij} (r_n^{\alpha\beta})_{ij}}{(r_n^{\alpha\beta})_{ij} + \eta^2} \cdot \frac{\partial W_{ij}}{\partial x^\alpha} \right), \quad (34)$$

3.3 SPH based on solid mechanics

In this section, SPH method is introduced to model the soil in the framework of solid mechanics. After applying SPH interpolation theory into the general equation of motion, the momentum equation can be expressed as:

$$\frac{D\mathbf{v}_i^\alpha}{Dt} = \sum_j m_j \left(\frac{\sigma_i^{\alpha\beta}}{\rho_i^2} + \frac{\sigma_j^{\alpha\beta}}{\rho_j^2} \right) \frac{\partial W_{ij}}{\partial x^\beta} + \mathbf{g}^\alpha, \quad (35)$$

The stress-strain relationship in SPH formulation can be immediately expressed as follows:

$$\frac{D\sigma^{\alpha\beta}}{Dt} = 2G \dot{\epsilon}_i^{\alpha\beta} + K \dot{\epsilon}_i^{\gamma\gamma} \delta_i^{\alpha\beta}, \quad (36)$$

and the strain rate tensor of a particle has discretized into the SPH formulations as:

$$\dot{\epsilon}_i^{\alpha\beta} = \frac{1}{2} \left(\frac{\partial v_i^\alpha}{\partial x_i^\beta} + \frac{\partial v_i^\beta}{\partial x_i^\alpha} \right) = \frac{1}{2} \left[\sum_j \frac{m_j}{\rho_j} (\mathbf{v}_j^\alpha - \mathbf{v}_i^\alpha) \cdot \frac{\partial W_{ij}}{\partial x_i^\beta} + \sum_j \frac{m_j}{\rho_j} (\mathbf{v}_j^\beta - \mathbf{v}_i^\beta) \cdot \frac{\partial W_{ij}}{\partial x_i^\alpha} \right] \quad (37)$$

3.3.1 Artificial viscosity

In the numerical solutions, unphysical oscillations are appearing if the dissipative term is not introduced into the governing equations. To improve the numerical stability and to

damp out such undesirable oscillations, artificial viscosity Π_{ij} is introduced into the momentum equation as follows:

$$\frac{D\mathbf{v}_i^\alpha}{Dt} = \sum_j m_j \left(\frac{\sigma_i^{\alpha\beta}}{\rho_i^2} + \frac{\sigma_j^{\alpha\beta}}{\rho_j^2} - \Pi_{ij} \delta_i^{\alpha\beta} \right) \frac{\partial W_{ij}}{\partial x^\beta} + g^\alpha, \quad (38)$$

The artificial viscosity Π_{ij} is derived by [Monaghan (1992)] as:

$$\Pi_{ij} = \begin{cases} \frac{-\alpha_\Pi C_{ij} \phi_{ij} + \beta_\Pi \phi_{ij}^2}{\rho_{ij}}, & \mathbf{v}_{ij} \cdot \mathbf{x}_{ij} < 0 \\ 0, & \mathbf{v}_{ij} \cdot \mathbf{x}_{ij} \geq 0 \end{cases} \quad (39)$$

where,

$$\phi_{ij} = \frac{h \mathbf{v}_{ij} \cdot \mathbf{r}_{ij}}{|\mathbf{r}_{ij}|^2 + \eta^2}, \quad C_{ij} = \frac{C_i + C_j}{2}, \quad \rho_{ij} = \frac{\rho_i + \rho_j}{2} \quad (40)$$

$$\mathbf{r}_{ij} = \mathbf{r}_i - \mathbf{r}_j, \quad \mathbf{v}_{ij} = \mathbf{v}_i - \mathbf{v}_j$$

In the above equation, α_Π and β_Π are constants and are chosen according to particular applications; C is the sound speed in soil, which is calculated from elastic bulk modulus and density as $C = \sqrt{K/\rho}$.

3.3.2 Tensile instability and artificial stress method

In the case of applied SPH in solids, the SPH particles mimic the behavior of the atoms. The instability, which is strictly related to the interpolation technique of the standard SPH method [Rabczuk, Belytschko and Xiao (2004)], is especially noticeable when simulating tension states in solids. The SPH particles forming clumps and causing non-physical fractures in the material. To avoid particles clumping, the artificial stress was proposed by Gray et al. [Gray, Monaghan and Swift (2001)] to eliminate the effects of tensile instability. The key idea of artificial stress is to introduce a small repulsive force between neighboring particles to avoiding particles clumping. Rabczuk et al. [Rabczuk and Belytschko (2007)] avoided instabilities in simulating the cracks by 3D-meshfree particle method.

In the current work, the artificial stress is introduced in three dimensions as follows:

$$\frac{D\mathbf{v}_i^\alpha}{Dt} = \sum_j m_j \left(\frac{\sigma_i^{\alpha\beta}}{\rho_i^2} + \frac{\sigma_j^{\alpha\beta}}{\rho_j^2} - \Pi_{ij} \delta_i^{\alpha\beta} + f_{ij}^n (R_i^{\alpha\beta} + R_j^{\alpha\beta}) \right) \frac{\partial W_{ij}}{\partial x^\beta} + g^\alpha, \quad (41)$$

where, n is the exponent dependent on the smoothing kernel and f_{ij} is the repulsive force term and is specified, according to Monaghan [Monaghan (2000)], in terms of the kernels as:

$$f_{ij} = \frac{W_{ij}}{W(\Delta d, h)} \quad (42)$$

where Δd is the initial particle spacing. h is assumed to be constant in the current work.

4 Results and discussions

In this section, the numerical examples have been introduced to validate the current scheme. In addition, several numerical tests for water-soil-solid interactions were performed.

4.1 Water/soil-suspension flow

The Louvain erosional dam break experiment presented by Fraccarollo et al. [Fraccarollo and Chapart (2002)] is used to validate the suspension model. Fig. 3 introduces the initial diagram of the Louvain erosional dam break experiment. The model has the following dimensions; width of the water is $L_w=1$ m and height $H_w=0.1$ m. The width of the soil bed is $L_s=2$ m and height $H_s=0.6$ m. The ratio of the density between soil and water is 1.54.

The collapse of the water column induces a surge leading to erosions of the soil. A suspension layer form between the pure soil and fluid whose evolution has been tracked in the experiments. Fig. 4 shows the evolution of the three phases in the experiment and the simulations at times 0.25, 0.5, 0.75 and 1.0 sec, respectively. Two simulations are considered in the comparison. The first simulation refers to suspension layers nested between water and soil. The second simulation is performed without a special treatment of the suspension layer. From the current investigation, the simulation with suspension layer gives more accurate validations compare to the experiment. While, the simulation without suspension layer has delay on the wave front of the water over soil compare to the experimental results and suspension case.

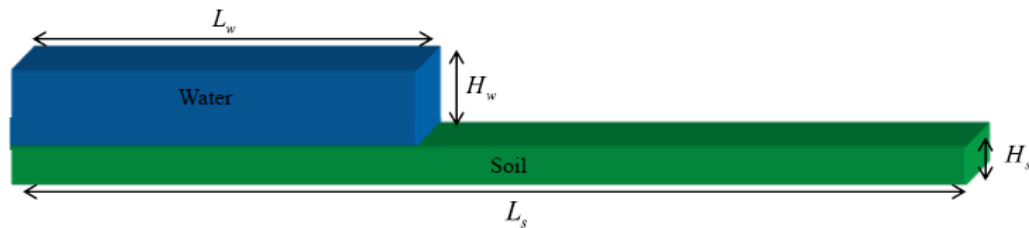
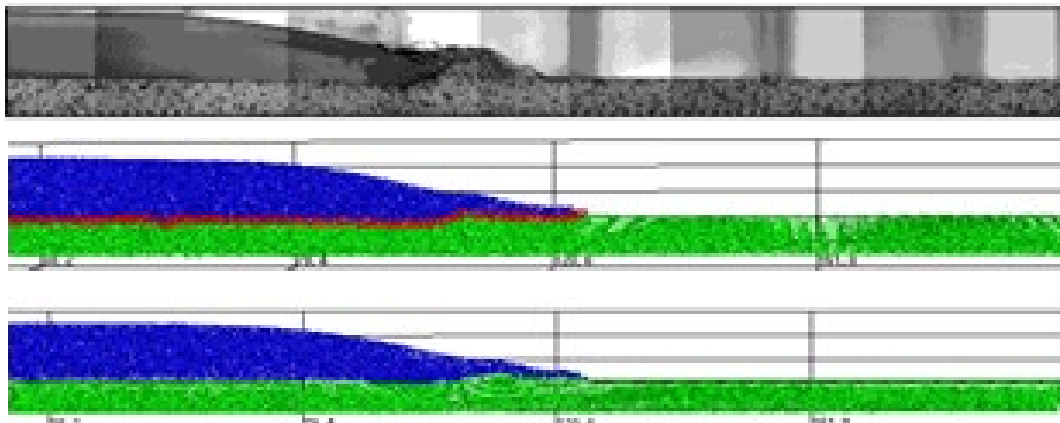
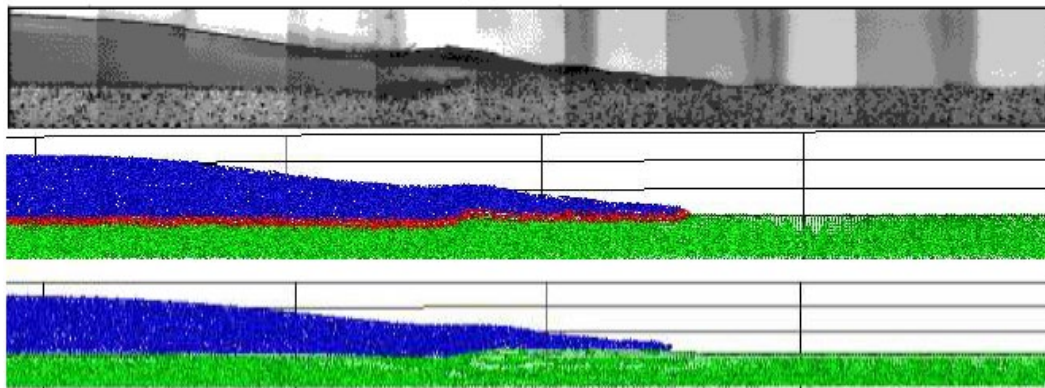


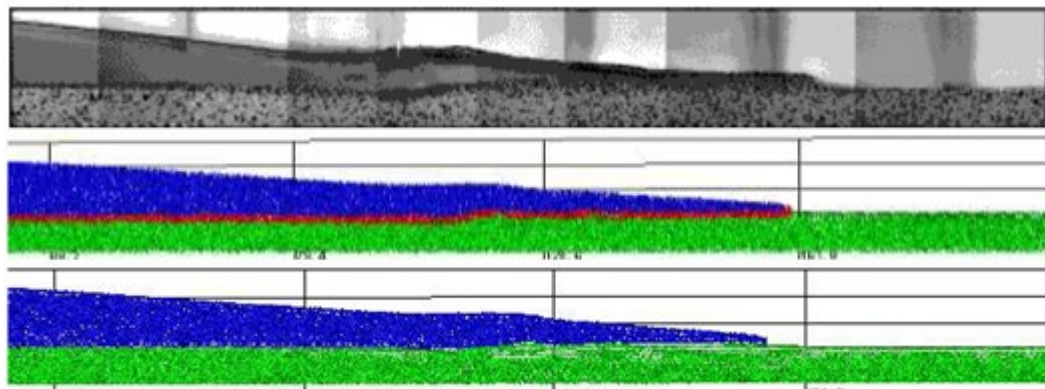
Figure 3: Initial schematic model of the Louvain erosional dam break experiment [Fraccarollo and Chapart (2002)]



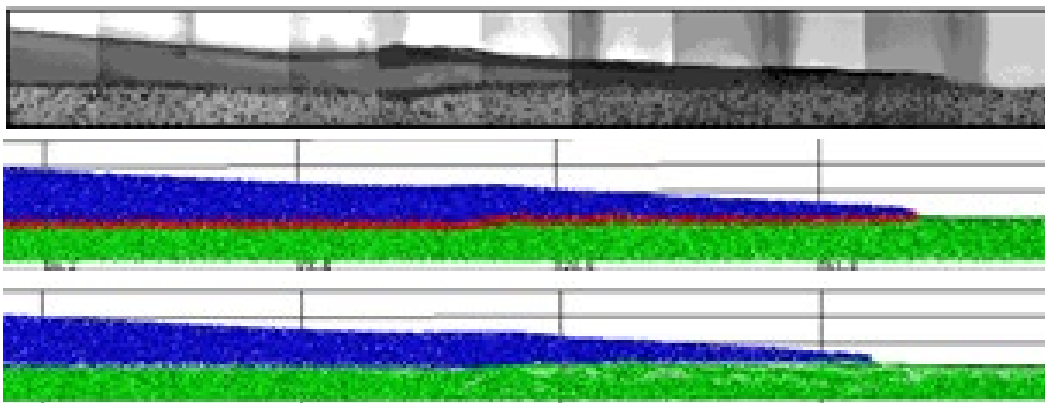
(a) $T=0.25$ sec



(b) T=0.5 sec



(c) T=0.75 sec



(d) T=1.0 sec

Figure 4: Comparison of dam break between experiment [Fraccarollo and Chapart (2002)] and simulations using current ISPH method at times 0.25 and 1.0 sec

4.2 Water-soil-solid interactions

Here, water, soil and solid interactions are introduced. To simulate soil hump, Bingham flow for seawall is not enough since the soil is modeled as a fluid with a variable viscosity, which leads to very soft soil even if the physical parameters are chosen with high values. Solid approach for soil is applied to simulate soil hump. The initial models for coupling between water-soil interactions with fully structure body and structure body over soil hump were introduced in Fig. 5. Here, the density of the structure body is taken as $\rho_3 = 2.8 \text{ gm/cm}^3$. In Fig. 6, the suspension layers are formed between the water and soil. After impact to the structure body, the splash waves of the water are formed over the structure. Later, the fluid flow makes an erosion behind the structure. Similar tendencies occur between the fluid-soil and structure over soil hump in Fig. 7. The only difference here appears after erosion in the soil hump. This simulation can predict the effects of the soil erosion in a dam break analysis. Additional numerical tests were presented in Figs. 8-10. The effects of the water flow velocity on both of the shape of the waves over structure and formed erosion around structure are presented in Fig. 8. It is observed that the shape of the wave over structure is strongly affected by the initial velocity of the fluid flow. Moreover, an extra erosion occurs near to the structure at low initial velocity of the fluid flow. One simulation trying to prevent erosion near to the structure is showed in Fig. 9. In this simulation, an extended structure behind the main structure was added to prevent erosion. Another simulation which tries to prevent the impact of the erosion by adding a wedge for the structure is shown in Fig. 10. In this case, the wedge can prevent the effects of the erosion around the structure during the fluid impacts.

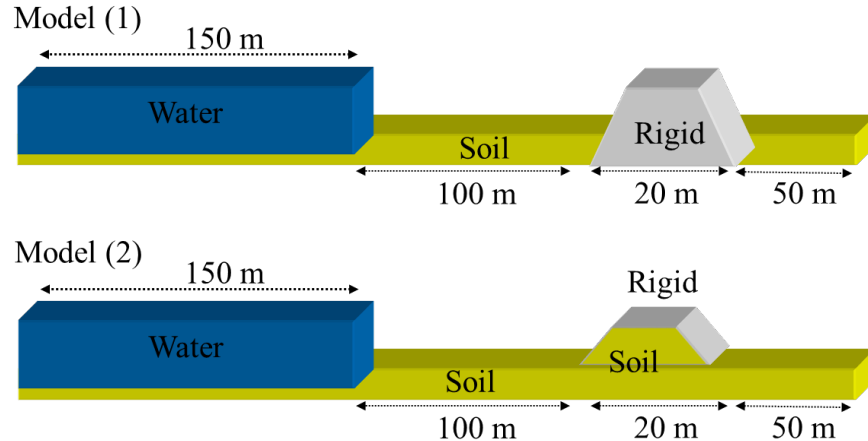


Figure 5: Initial schematic diagrams of models 1 and 2

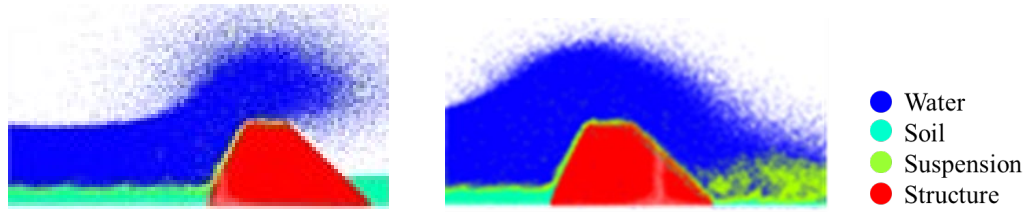


Figure 6: Coupling between water-soil interactions with structure body

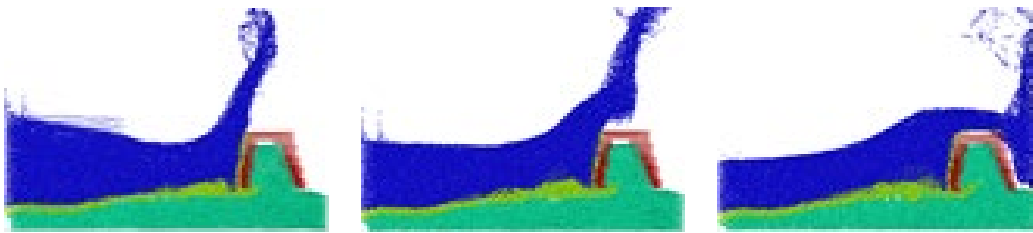
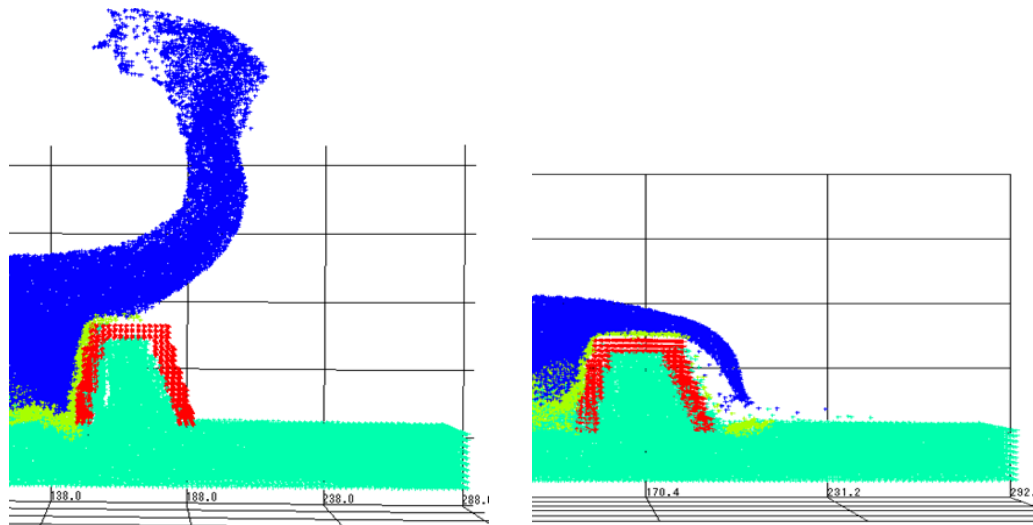
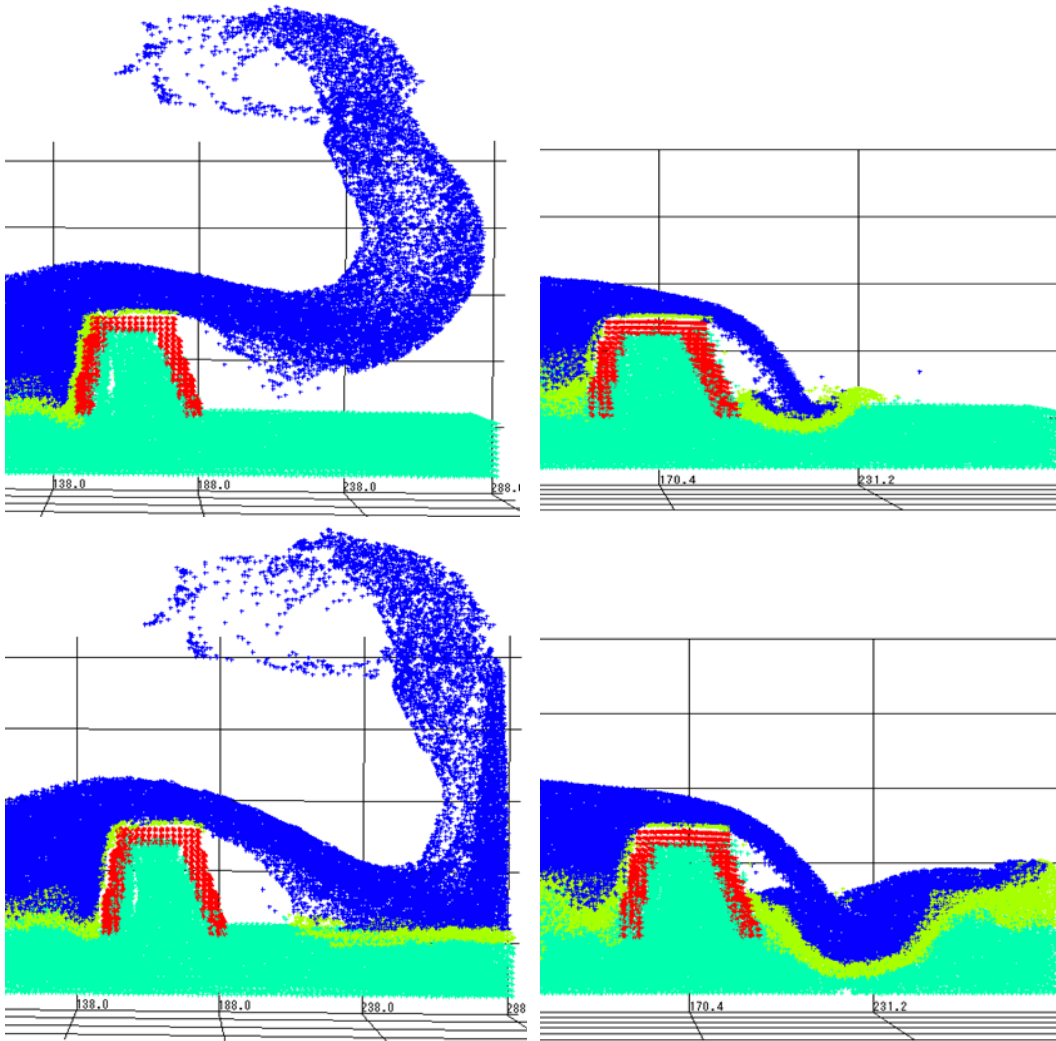


Figure 7: Coupling between water-soil interactions with structure body over soil hump

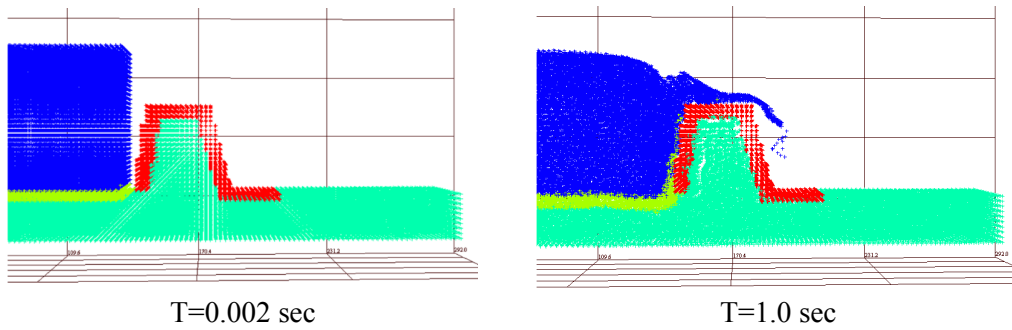




(a) High initial velocity

(b) Low initial velocity

Figure 8: Coupling between water-soil-solid interactions with two different initial velocity



T=0.002 sec

T=1.0 sec

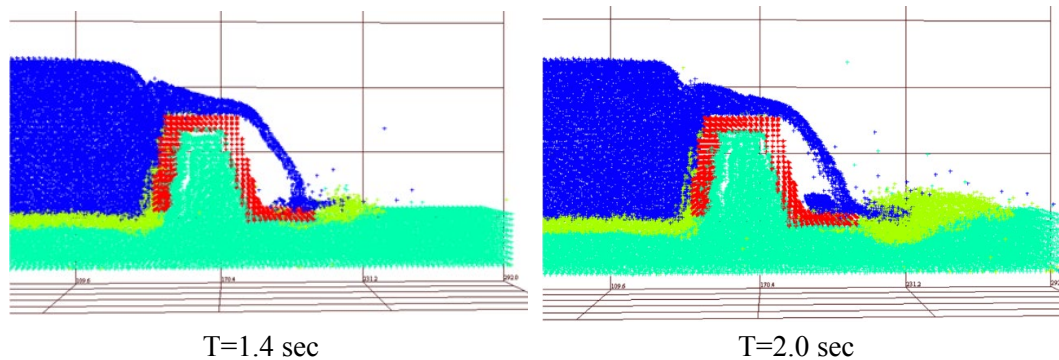


Figure 9: Coupling between water-soil-solid interactions with extended solid structure

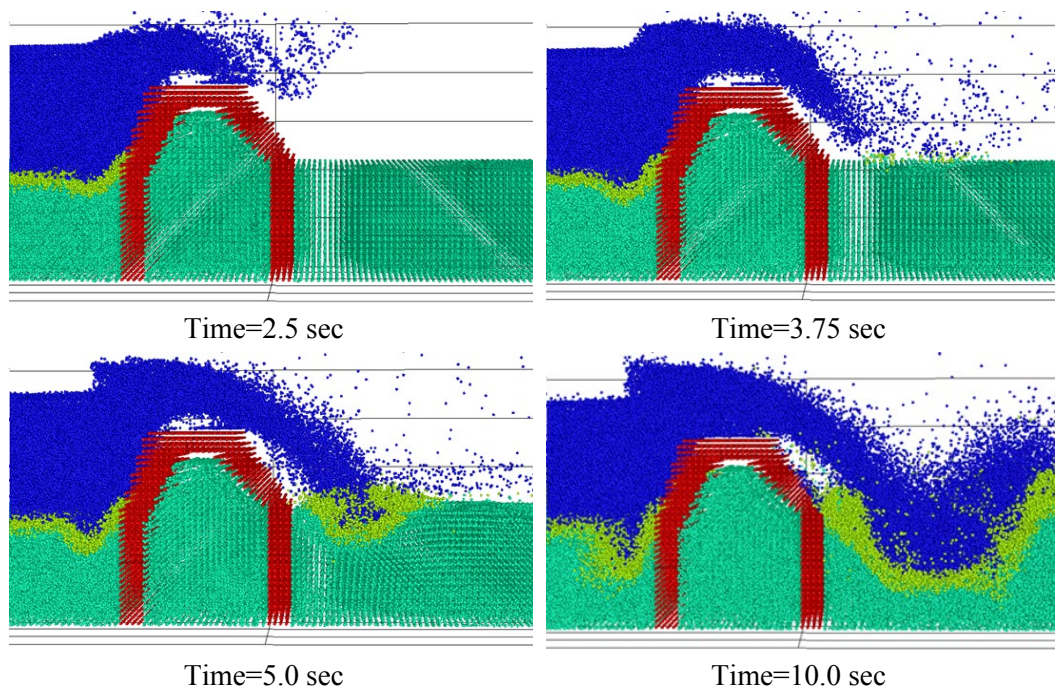


Figure 10: Coupling between water-soil-solid interactions with wedge structure

5 Conclusion

In this study, an ISPH method has been used to simulate water, soil and solid structure interactions. The fluid is modeled as a Newtonian fluid and the soil is modeled in two different cases depending on the nature of the simulation. Firstly, the soil is simulated by Bingham model. In this model, the granular material is taken as a fluid with derived viscosity from the cohesion and friction angle. Moreover, the Bingham type constitutive model is proposed based on Mohr-Coulomb yield-stress criterion. From the validation with the experimental results, the simulation with suspension layer gives more accurate validations compare to the experiment.

Secondly, the soil is modeled by the solid mechanics, and the soil constitutive model is based on the Hooke's law of linear elasticity. The nested suspension layers between water and soil are formed in both of the two cases.

From the current simulations, the following points are reported:

- The shape of the wave over structure is strongly depend on the initial velocity of the fluid flow.
- An extra erosion occurs near to the structure at a low initial velocity of the fluid flow.
- An extended structure behind the main structure try to prevent erosion.
- Adding a wedge can prevent the structure from the impact of the erosion.

Finally, the solid structure is taken as a rigid body in this study and as a future work, the solid structure will be taken as a concrete material with deformations.

Acknowledgement: The authors would like to extend their appreciations to the Deanship of Scientific Research at King Khalid University, Abha, Saudi Arabia, for funding this work through the Research Group Project under grant number (R. G. P2/70/41).

Funding Statement: This work was supported by Deanship of Scientific Research at King Khalid University, Abha, Saudi Arabia, through the Research Group Project under grant number R.G.P2/70/41.

Conflicts of Interest: The authors declare that they have no conflicts of interest to report regarding the present study.

References

- Aly, A. M.; Asai, M.; Sonoda, Y.** (2011): Modelling of surface tension force for free surface flows in ISPH method. *International Journal of Numerical Methods for Heat & Fluid Flow*, vol. 23, no. 3, pp. 479-498.
- Aly, A. M.; Asai, M.; Sonoda, Y.** (2011): Simulation of free falling rigid body into water by a stabilized incompressible SPH method. *Ocean Systems Engineering, an International Journal*, vol. 1, no. 3, pp. 207-222.
- Asai, M.; Aly, A. M.; Sonoda, Y.; Sakai, Y.** (2012): A Stabilized incompressible SPH method by relaxing the density invariance condition. *Journal of Applied Mathematics*, vol. 2012, pp. 1-24.
- Bui, H. H.; Fukagawa, R.** (2013): An improved SPH method for saturated soils and its application to investigate the mechanisms of embankment failure: case of hydrostatic pore-water pressure. *International Journal for Numerical and Analytical Methods in Geomechanics*, vol. 37, pp. 31-50.
- Bui, H. H.; Fukagawa, R.; Sako, K.; Ohno, S.** (2008): Lagrangian mesh-free particle method (SPH) for large deformation and post-failure of geomaterial using elastic-plastic soil constitutive model. *International Journal for Numerical and Analytical Methods in Geomechanics*, vol. 32, no. 12, pp. 1537-1573.
- Bui, H. H.; Sako, K.; Fukagawa, R.** (2007): Numerical simulation of soil-water

interaction using smoothed particle hydrodynamics (SPH) method. *Journal of Terramechanics*, vol. 44, no. 5, pp. 339-346.

Chorin, A. J. (1968): Numerical solution of the Navier-Stokes equations. *Mathematics of Computation*, vol. 22, pp. 745-762.

Cummins, S. J.; Rudman, M. (1999): An SPH projection method. *Journal of Computational Physics*, vol. 152, no. 2, pp. 584-607.

Dai, Z.; Ren, H.; Zhuang, X.; Rabczuk, T. (2017): Dual-support smoothed particle hydrodynamics for elastic mechanics. *International Journal of Computational Methods*, vol. 14, no. 4, 1750039.

Ellero, M.; Serrano, M.; Espanol, P. (2007): Incompressible smoothed particle hydrodynamics. *Journal of Computational Physics*, vol. 226, pp. 1731-1752.

Fraccarollo, L.; Chapart, H. (2002): Riemann wave description of erosional dam-break flows. *Journal of Fluid Mechanics*, vol. 461, pp. 183-228.

Gingold, R. A.; Monaghan, J. J. (1977): Smoothed particle hydrodynamics: theory and application to non-spherical stars. *Monthly Notices of the Royal Astronomical Society*, vol. 181, pp. 375-389.

Gray, J. P.; Monaghan, J. J.; Swift, R. P. (2001): SPH elastic dynamics. *Computer Methods in Applied Mechanics and Engineering*, vol. 190, pp. 6641-6262.

Hu, X. Y.; Adams, N. A. (2006): Angular-momentum conservative smoothed particle dynamics for incompressible viscous flows. *Physics Fluids*, vol. 18, pp. 101702-101704.

Hu, X. Y.; Adams, N. A. (2007): An incompressible multi-phase SPH method. *Journal of Computational Physics*, vol. 227, pp. 264-278.

Hu, X. Y.; Adams, N. A. (2009): A constant-density approach for incompressible multi-phase SPH. *Journal of Computational Physics*, vol. 228, pp. 2082-2091.

Khayyer, A.; Gotoh, H.; Shao, S. (2008): Corrected incompressible SPH method for accurate water-surface tracking in breaking waves. *Coastal Engineering*, vol. 55, pp. 236-250.

Khayyer, A.; Gotoh, H.; Shao, S. (2009): Enhanced predictions of wave impact pressure by improved incompressible SPH methods. *Applied Ocean Research*, vol. 31, pp. 111-131.

Lee, E. S.; Moulinec, C.; Xu, R.; Violeau, D.; Laurence, D. et al. (2008): Comparisons of weakly compressible and truly incompressible algorithms for the SPH mesh free particle method. *Journal of Computational Physics*, vol. 18, pp. 8417-8436.

Lucy, L. B. (1977): A numerical approach to the testing of the fusion process. *Astronomy Journal*, vol. 88, pp. 1013-1024.

Monaghan, J. J. (1992): Smoothed particle hydrodynamics. *Annual Review of Astronomy and Astrophysics*, vol. 30, pp. 543-574.

Monaghan, J. J. (1994): Simulating free surface flows with SPH. *Journal of Computational Physics*, vol. 110, pp. 399-406.

Monaghan, J. J. (1995): Heat conduction with discontinuous conductivity. *Applied Mathematics Reports and Preprints, Monash University*.

Monaghan, J. J. (2000): SPH without a tensile instability. *Journal of Computational*

Physics, vol. 159, pp. 290-311

Morris, J. P.; Fox, P. J.; Zhu, Y. (1997): Modeling low reynolds number incompressible flows using SPH. *Journal of Computational Physics*, vol. 136, pp. 214-226.

Okahci, N.; Hirota, A.; Izawa, S.; Fukunishi, Y.; Higuchi, H. (2001): SPH simulation of pulsating pipe flow at a junction. *Proceedings of 1st International Symposium on Advanced Fluid Information*, pp. 388-391.

Pastor, M.; Haddad, B.; Sorbino, G.; Cuomo, S.; Drempetic, V. (2009): A depth-integrated, coupled SPH model for flow-like landslides and related phenomena. *International Journal for Numerical and Analytical Methods in Geomechanics*, vol. 33, pp. 43-172.

Pozorski, J.; Wawrenczuk, A. (2002): SPH computation of incompressible viscous flows. *Theoretical Applied Mechanics*, vol. 40, pp. 917-937.

Rabczuk, T.; Belytschko, T. (2007): A three-dimensional large deformation meshfree method for arbitrary evolving cracks, *Computer Methods in Applied Mechanics and Engineering*, vol. 196, no. 29-30, pp. 2777-2799.

Rabczuk, T.; Ren, H.; Zhuang, X. (2019): A nonlocal operator method for partial differential equations with application to electromagnetic waveguide problem. *Computers, Materials and Continua*, vol. 59, no. 1, pp. 31-55.

Ren, H.; Zhuang, X.; Cai, Y.; Rabczuk, T. (2016): Dual-horizon peridynamics. *International Journal for Numerical Methods in Engineering*, vol. 108, pp. 1451-1476.

Ren, H.; Zhuang, X.; Rabczuk, T. (2017): Dual-horizon peridynamics: a stable solution to varying horizons. *Computer Methods in Applied Mechanics and Engineering*, vol. 318, pp. 762-782.

Ren, H.; Zhuang, X.; Rabczuk, T. (2019): A dual-support smoothed particle hydrodynamics for weakly compressible fluid inspired by the dual-horizon peridynamics. *Computer Modeling in Engineering & Sciences*, vol. 121, no. 2, pp. 353-383.

Ren, H.; Zhuang, X.; Rabczuk, T.; Zhu, H. (2019): Dual-support smoothed particle hydrodynamics in solid: variational principle and implicit formulation, *Engineering Analysis with Boundary Elements*, vol. 108, pp. 15-29.

Shao, S.; Lo, E. Y. M. (2003): Incompressible SPH method for simulating Newtonian and non-Newtonian flows with a free surface. *Advances in Water Resources*, vol. 26, pp. 787-800.

Ulrich, C.; Koliha, N.; Rung, T. (2011): SPH modelling of water/soil flows using a variable resolution scheme. *Proceeding of the 6th International SPHERIC Workshop*, pp. 101-108.

Violeau, D.; Issa, R. (2007): Numerical modelling of complex turbulent free-surface flows with the SPH method: an overview. *International Journal of Numerical Methods in Fluids*, vol. 53, pp. 277-304.